A Hybrid Analytical Approximate Technique for Solving Transient Natural Convection in a Horizontal Concentric Cylinders

Yasir Ahmed Abdulameer*, Abdul-Sattar Jaber Ali Al-Saif

Department of Mathematics, College of Education for Pure Science, University of Basrah, Basra, Iraq.

*Corresponding author E-mail: pepg.yasir.ahmed@uobasrah.edu.iq

Doi: 10.29072/basjs.20230104

ARTICLE INFO

Keywords

Homotopy perturbation method, Fourier transform, Natural convection, Cylindrical annuli, Convergence analysis

ABSTRACT

A hybrid procedure combining the homotopy perturbation method and the Fourier transform has been proposed, and it was used to find an approximate analytical solution to the problem of two-dimensional transient natural convection in a horizontal cylindrical concentric annulus bounded by two isothermal surfaces. The effect of varying values of the Grashof number, Prandtl number, and radius ratio on fluid flow (air) and heat transfer is explored. Furthermore, the velocity distributions and the average Nusselt number are investigated, with Nusselt numbers utilized to express local and global heat transfer rates. Finally, the convergence of the new algorithm was theoretically checked by proving several theorems, which were then applied to the findings of the new solutions provided by the suggested approach.

Received 14 Jan 2022; Received in revised form 13 March 2023; Accepted 12 Apr 2023, Published 30 Apr 2023

1. Introduction

Recently, researchers and scientists have been interested in studying the theory of heat transfer by natural convection because of its wide applications in various fields of science and technology. These applications include aircraft cabin insulation, nuclear reactors, solar collector sensors, heat storage systems, power transmission cables, cooling of electronic components, etc. [1, 8, 11, 17, 19]. One of the most famous problems of natural convection that has attracted the attention of quite a few researchers is the problem of two-dimensional transient natural convection between two concentric circular horizontal cylinders. Among the first researchers who contributed to providing experimental solutions to the problem of natural convection between two horizontal concentric cylinders are Crawford and Limlich [3], who carried out a numerical study in order to find solutions to this problem, during this study they succeeded in approximating the steady-state differential equations with appropriate difference equations, moreover, the effect of diameter ratios at 2, 8 and 57 is discussed in the case of Prandtl number 0.7. This study paved the way for many authors and researchers who succeeded in finding numerical and analytical solutions to the mentioned problem, for example, Lawrence et al. [9] presented an analytical study in which they used the Rayleigh number power series to solve the problem of natural convection between two concentric horizontal cylinders with slight temperature difference. During their study, the effect of Prandtl number, Rayleigh number and radius ratio on streamline formation, local heat transfer rates, velocity and temperature distributions were discussed. Experimental and theoretical-numerical studies were introduced by Kuehn and Goldstein [8]. Mach-Zehnder interferometer uas used in experimentally study to locate temperature distributions and coefficients of local heat-transfer. On the other hand, the governing invariant property equations have been solved numerically relying on the finite difference method. Their comparisons between experimental and numerical results under similar conditions illustrated good agreement. Tsui and Tremblay [17] contributed to a theoretical-numerical study in which they discussed the effect of Grashof number from 7×10^2 to 9×10^4 as well as the effect of Variation in diameter ratio between 1.2, 1.5 and 2 when Prandtl number is fixed at 0.7. Pop et. al. [12] obtained an approximate analytical solutions to the presented problem, they used the method of matched asymptotic expansions, through which they were able to obtain the solutions for three regions (inner boundary layer, core and outer boundary layer) to short times, and they found that the solution is clearly distinct from the solution of the steady state. Hassan and Al-Lateef [7] conducted a numerical study in which the energy and vorticity equation was solved using the alternating direction implicit (ADI) method, while the

stream function equation was solved using the successive over relaxation (SOR) method. The results of the numerical solutions were discussed based on the difference in diameter ratio between 1.2, 1.5 and 2 as well as the effect of difference in the Grashof number from 10^2 to 10^5 with a difference in the Prandtl number values. A numerical study of natural convection in a horizontal annulus with two heating blocks has been presented by Touzani et. al. [18], they found that heat transfer increases significantly at the upper region of the annulus, in addition, they note that the presence of block helps to improve the heat transfer in general. A new procedure based on combining the homotopy perturbation method and Yang transform was proposed by Al-Saif and Al-Griffi [2], who succeeded in finding analytical approximate solutions to the problem of two-dimensional transient natural convection in a concentric cylindrical horizontal annulus bounded by two isothermal surfaces. During their work the effect of different values of each of the Grashof number and the radius ratio on heat transfer and fluid flow (air) at Prandtl number 0.7 was studied.

Despite the capabilities of many iterative methods and the possibility of their application in order to find analytical solutions to non-linear flow problems, especially the problems of natural convection, most of these methods are almost not without some difficulties resulting from high computational operations that require great time and effort in order to obtain the desired solution to the studied problem, such as HPM [10], HAM [13] and DQ method [14,16]. As well as, it is possible to rely on various integral transformations (Yang transform, Laplace transform, Fourier transform, ...) in finding analytical solutions to linear problems, but it is often difficult to apply these transformations to obtain analytical solutions to some non-linear problems. What was mentioned prompts us to create a new procedure by which we can avoid the mentioned difficulties. In recent years, researchers have noted that a combining of integrative transform methods and iterative methods may help address the difficulties that arise when applying each method individually. Moreover, we proposed to combine the Fourier transform with the homotopy perturbation method (HPM) to get a new algorithm that we refer to as (FT-HPM). In addition to what we have mentioned, and as a result of our modest review of the previous literatures, we did not find anyone who has used this technique (FT-HPM) to solve the problems of natural convection, and in particular the current problem. In this work, a new developed algorithm (FT-HPM) is presented in order to find approximate analytical solutions to the two-dimensional transient natural convection problems in a concentric horizontal cylindrical annulus. Moreover, the problem was divided into three regions, the inner boundary layer (located near the inner

cylinder), the outer boundary layer (located near the outer cylinder), and core region located between the two layers, and depending on the proposed method, the analytical solutions were found for the mentioned regions. Besides what has been mentioned, we have studied the convergence analysis of the new method analytically and experimentally by formulating and proving some theorems. In addition, we have applied these theorems to the results of the obtained analytical solutions. The tables and graphs of the new analytical solutions show the necessity, importance and benefit of using the current method. In addition, the results showed the accuracy and efficiency of the new technique, and they are in agreement with the results of previously published studies [1, 7, 17].

2. Basic Idea of Homotopy Perturbation Method

In 1998, the homotopy perturbation method (HPM) was introduced by researcher He J. Huan [5, 6]. This method was characterized by its ability to solve many linear and non-linear differential and integral equations. This method is considered highly accurate and efficient and has proven effective in solving many non-linear problems that have wide applications in various fields of life. When using this method, the solution is assumed as the sum of an infinite convergent series [4]. To display the basic idea of this method, we must consider the general form of the following non-linear differential equation:

$$A(u) - g(r) = 0, r \in \Omega, \tag{1}$$

associated with the following boundary conditions:

$$B(u, \frac{\partial u}{\partial n}) = 0, r \in \Gamma, \tag{2}$$

Where u denotes to the unknown function, $g(r)$ is a known analytic function, A, B and Γ represent the general differential operator, boundary operator and the boundary of the domain Ω, respectively. The operator A can be divided into linear operator L and non-linear operator N. Moreover, Eq. (1) can be rewritten as:

$$L(u) + N(u) - q(r) = 0. \tag{3}$$

Through the basic idea of the homotopy perturbation method, the homotopy $U(r, p)$: $\Omega \times [0,1] \longrightarrow \mathbb{R}$ is defined by the following formula

$$H(U, p) = (1 - p)[L(U) - L(u_0)] + p[A(U) - g(r)] = 0, \tag{4}$$

Or

$$H(U,p) = L(U) - L(u_0) + pL(u_0) + p[N(U) - g(r)] = 0, \quad (5)$$

where $p \in [0,1]$ refers to the impeding parameter and u_0 is an initial solution of Eq. (1), which satisfies the boundary conditions of Eq. (2). It is clear that Eq. (4) or (5) satisfies the conditions of homotopy as follows

$$\left.\begin{aligned} H(U,0) &= L(U) - L(u_0) = 0, \\ H(U,1) &= A(U) - g(r) = 0\ . \end{aligned}\right\} \quad (6)$$

Now, the solution of Eq. (4 or 5) can be assumed as a power series for p as follows:

$$U = \sum_{j=0}^{\infty} p^j U_j \quad (7)$$

by setting $p = 1$, the approximate solution of Eq. (1) can be given as follows

$$u = \lim_{p\to 1} U = \sum_{j=0}^{\infty} U_j. \quad (8)$$

3. Basic Algorithm of FT-HPM

The fundamental idea of this section is to develop the homotopy perturbation method by using the Fourier transform in order to obtain a more advanced hybrid procedure. To give a full explanation of the new algorithm, we have to write the non-linear differential equation in the following form:

$$\frac{\partial^n}{\partial r_1^n}\left(\frac{\partial^m}{\partial r_2^m} U\right) + R(U) + N(U) = g(r_1, r_2)\ , r_1, r_2 \in \Omega, \quad (9)$$

where R and N represents the linear and non-linear differential operator, respectively, and $g(r_1, r_2)$ refers to the source term. Accordingly, we can view the basic steps of this algorithm as follows:

Taking the Fourier transform with respect to r_1 for both sides of Equation (9), we have

$$\mathcal{F}_1\left[\frac{\partial^n}{\partial r_1^n}\left(\frac{\partial^m}{\partial r_2^m} U\right)\right] + \mathcal{F}_1[R(U) + N(U) - g(r_1, r_2)] = 0\ ,\ r_1, r_2 \in \Omega. \quad (10)$$

Using the differentiation property of the Fourier transform, we obtain

$$(i\omega)^n \mathcal{F}_1\left[\frac{\partial^m}{\partial r_2^m} U\right] + \mathcal{F}_1[R(U) + N(U) - g(r_1, r_2)] = 0. \quad (11)$$

The rearrangement of Eq. (11) leads to

$$\mathcal{F}_1\left[\frac{\partial^m}{\partial r_2^m} U\right] + \frac{1}{(i\omega)^n}\mathcal{F}_1[R(U) + N(U) - g(r_1, r_2)] = 0. \quad (12)$$

Taking the inverse FT for both sides of Eq. (12), we get:

$$\frac{\partial^m}{\partial r_2^m}U + \mathcal{F}_1^{-1}\left[\frac{1}{(i\omega)^n}\mathcal{F}_1[R(U)+N(U)-g(r_1,r_2)]\right] = 0. \quad (13)$$

By using the HPM, we have

$$(1-p)\left[\frac{\partial^m}{\partial r_2^m}U - \frac{\partial^m}{\partial r_2^m}u_0\right] + p\left[\frac{\partial^m}{\partial r_2^m}U + \mathcal{F}_1^{-1}\left\{\frac{1}{(i\omega)^n}\mathcal{F}_1[R(U)+N(U)-g(r_1,r_2)]\right\}\right] = 0. \quad (14)$$

Rearrangement Eq. (14), we deduce

$$\frac{\partial^m}{\partial r_2^m}U = \frac{\partial^m}{\partial r_2^m}u_0 - p\frac{\partial^m}{\partial r_2^m}u_0 - p\left[\mathcal{F}_1^{-1}\left\{\frac{1}{(i\omega)^n}\mathcal{F}_1[R(U)+N(U)-g(r_1,r_2)]\right\}\right]. \quad (15)$$

by applying the Fourier transform with respect to r_2 on both sides of Eq. (15), we have

$$\mathcal{F}_2\left[\frac{\partial^m}{\partial r_2^m}U\right] = \mathcal{F}_2\left[\frac{\partial^m}{\partial r_2^m}u_0\right] - p\mathcal{F}_2\left[\frac{\partial^m}{\partial r_2^m}u_0 + \mathcal{F}_1^{-1}\left\{\frac{1}{(i\omega)^n}\mathcal{F}_1[R(U)+N(U)-g(r_1,r_2)]\right\}\right]. \quad (16)$$

where, $\mathcal{F}_k[g(r_k)] = \mathcal{F}_k(\omega) = \int_{-\infty}^{\infty} g(r_k)e^{-i\omega r_k}\,dr_k$, $k = 1,2$.

by the differentiation property of the Fourier transform, we get

$$\mathcal{F}_2[U] = \frac{1}{(i\omega)^m}\mathcal{F}_2\left[\frac{\partial^m}{\partial r_2^m}u_0\right] - \frac{p}{(i\omega)^m}\mathcal{F}_2\left[\frac{\partial^m}{\partial r_2^m}u_0 + \mathcal{F}_1^{-1}\left\{\frac{1}{(i\omega)^n}\mathcal{F}_1[R(U)+N(U)-g(r_1,r_2)]\right\}\right]. \quad (17)$$

Taking the inverse FT for both sides of Eq. (17), we have

$$U = \mathcal{F}_2^{-1}\left[\frac{1}{(i\omega)^m}\mathcal{F}_2\left[\frac{\partial^m}{\partial r_2^m}u_0\right]\right] - \mathcal{F}_2^{-1}\left[\frac{p}{(i\omega)^m}\mathcal{F}_2\left\{\frac{\partial^m}{\partial r_2^m}u_0 + \mathcal{F}_1^{-1}\left[\frac{1}{(i\omega)^n}\mathcal{F}_1\left\{\begin{matrix}R(U)+N(U)-\\ g(r_1,r_2)\end{matrix}\right\}\right]\right\}\right]. \quad (18)$$

From the assumption of the HPM, we have

$$U = \sum_{j=0}^{\infty} p^j U_j, \quad (19)$$

and the nonlinear terms can be decomposed as

$$N(U) = \sum_{j=0}^{\infty} p^j H_j. \quad (20)$$

Where $H_j(U)$ represent the He's polynomials [15] that are given by:

$$H_j(U_0, U_1, U_2, \ldots, U_j) = \frac{1}{j!}\frac{\partial^j}{\partial p^j}\left[N\left(\sum_{i=0}^{\infty} p^i U_i\right)\right]_{p=0}, j = 0,1,2,3, \ldots \quad (21)$$

Putting Eq_s. (19) and (20) in to Eq. (18), we obtain

$$\sum_{j=0}^{\infty} p^j U_j = \mathcal{F}_2^{-1}\left[\begin{matrix}\frac{1}{(i\omega)^m}\mathcal{F}_2\left[\frac{\partial^m}{\partial r_2^m}u_0\right] - \frac{p}{(i\omega)^m}\mathcal{F}_2\left[\frac{\partial^m}{\partial r_2^m}u_0\right] - \\ \frac{p}{(i\omega)^m}\mathcal{F}_2\left[\mathcal{F}_1^{-1}\left\{\frac{1}{(i\omega)^n}\mathcal{F}_1\left[R\left(\sum_{j=0}^{\infty} p^j U_j\right) + \sum_{j=0}^{\infty} p^j H_j - g(r_1,r_2)\right]\right\}\right]\end{matrix}\right]. \quad (22)$$

By comparing the coefficients of the same powers of p, we get

$$p^0: U_0 = \mathcal{F}_2^{-1}\left[\frac{1}{(i\omega)^m}\mathcal{F}_2\left[\frac{\partial^m}{\partial r_2^m}u_0\right]\right], \tag{23}$$

$$p^1: U_1 = \mathcal{F}_2^{-1}\left[-\frac{1}{(i\omega)^m}\mathcal{F}_2\left[\frac{\partial^m}{\partial r_2^m}u_0\right] - \frac{1}{(i\omega)^m}\mathcal{F}_2\left[\mathcal{F}_1^{-1}\left\{\frac{1}{(i\omega)^n}\mathcal{F}_1[R(U_0) + H_0 - g(r_1, r_2)]\right\}\right]\right], \tag{24}$$

$$p^2: U_2 = \mathcal{F}_2^{-1}\left[-\frac{1}{(i\omega)^m}\mathcal{F}_2\left[\mathcal{F}_1^{-1}\left\{\frac{1}{(i\omega)^n}\mathcal{F}_1[R(U_1) + H_1]\right\}\right]\right], \tag{25}$$

$$\vdots$$

$$p^j: U_j = \mathcal{F}_2^{-1}\left[-\frac{1}{(i\omega)^m}\mathcal{F}_2\left[\mathcal{F}_1^{-1}\left\{\frac{1}{(i\omega)^n}\mathcal{F}_1\left[R\left(U_{j-1}\right) + H_{j-1}\right]\right\}\right]\right], \tag{26}$$

Taking $p = 1$, then the analytical approximate solution u can be given by

$$u = \lim_{p\to 1} U = \sum_{j=0}^{\infty} U_j. \tag{27}$$

4. Mathematical formulation of governing equation

We consider the Newtonian fluid in two concentric horizontal circular cylinders enclosed by two isothermal surfaces. The problem is formulated in Fig. (1) as follows: (a) both fluid motion and temperature distribution are chosen as two-dimensional (2-D), (b) fluid is incompressible in addition to being viscous, (c) the friction heating is almost too slight, and (c) the properties of fluid are constant except that density changes with temperature. Therefore, the governing mathematical equations can be presented by the Boussinesq approximation by the following formulas [17]:

$$\frac{\partial \hat{U}}{\partial \hat{x}} + \frac{\partial \hat{V}}{\partial \hat{y}} = 0, \tag{28}$$

$$\frac{\partial \hat{U}}{\partial \hat{t}} + \hat{U}\frac{\partial \hat{U}}{\partial \hat{x}} + \hat{V}\frac{\partial \hat{U}}{\partial \hat{y}} = \left(\frac{-1}{\rho}\right)\frac{\partial \hat{P}}{\partial \hat{x}} + \hat{v}\left(\frac{\partial^2 \hat{U}}{\partial \hat{x}^2} + \frac{\partial^2 \hat{U}}{\partial \hat{y}^2}\right), \tag{29}$$

$$\frac{\partial \hat{V}}{\partial \hat{t}} + \hat{U}\frac{\partial \hat{V}}{\partial \hat{x}} + \hat{V}\frac{\partial \hat{V}}{\partial \hat{y}} = \left(\frac{-1}{\rho}\right)\frac{\partial \hat{P}}{\partial \hat{y}} + \hat{v}\left(\frac{\partial^2 \hat{V}}{\partial \hat{x}^2} + \frac{\partial^2 \hat{V}}{\partial \hat{y}^2}\right) + \hat{g}\hat{\alpha}\left(\hat{T} - \hat{T}_o\right), \tag{30}$$

$$\frac{\partial \hat{T}}{\partial \hat{t}} + \hat{U}\frac{\partial \hat{T}}{\partial \hat{x}} + \hat{V}\frac{\partial \hat{T}}{\partial \hat{y}} = \hat{k}\left(\frac{\partial^2 \hat{T}}{\partial \hat{x}^2} + \frac{\partial^2 \hat{T}}{\partial \hat{y}^2}\right), \tag{31}$$

where; $\hat{U}$, $\hat{V}$ refer to the components of velocity in $\hat{x}$, $\hat{y}$ directions; $\hat{T}$, $\hat{g}$, $\hat{v}$, ρ, $\hat{\alpha}$ and $\hat{k}$ indicate to temperature, gravity acceleration, kinematic viscosity, density, thermal expansion coefficient, and thermal diffusivity, respectively.

In order to facilitate the solution of the problem, we can reduce Eqs. (29) and (30) to the vorticity-stream form by differentiating Eq. (29) with respect to $\hat{y}$ and Eq. (30) with respect to $\hat{x}$, then one of the two equations is subtracted from the other and using the definition of the vorticity function $\left(\hat{\mathcal{G}} = \frac{\partial \hat{V}}{\partial \hat{x}} + \frac{\partial \hat{U}}{\partial \hat{y}}\right)$, the pressure is omitted. In addition, the Cartesian coordinate system is converted to the polar coordinate system. Then the problem is converted from the dimensional form to the non-dimensional form using the dimensionless set as the following:

$$U = \frac{\hat{U}\hat{L}}{\hat{v}}\ ,\ V = \frac{\hat{V}\hat{L}}{\hat{v}}\ ,\ \psi = \frac{\hat{\psi}}{\hat{v}}\ ,r = \frac{\hat{r}}{\hat{L}}\ ,\ t = \frac{\hat{t}\hat{v}}{\hat{L}^2}\ ,\ \mathcal{G} = \frac{\hat{L}^2\hat{\mathcal{G}}}{\hat{v}}\ ,\ T = \frac{\hat{T}-\hat{T}_o}{\hat{T}_h-\hat{T}_c}\ ,\ \nabla^2 = \hat{L}^2\hat{\nabla}^2. \tag{32}$$

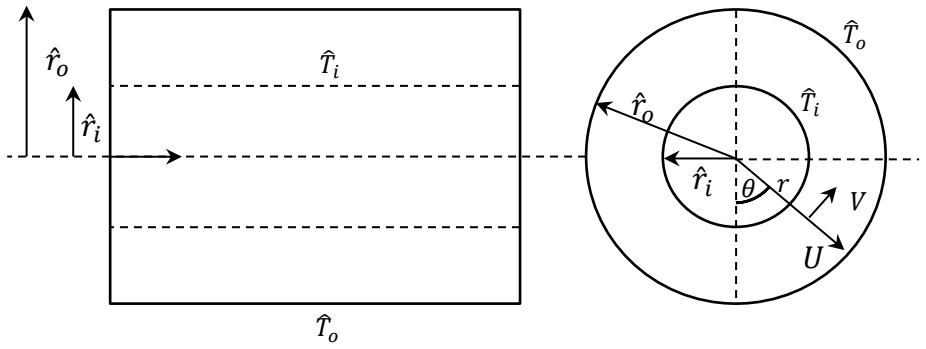

Figure 1: Physical flow geometry and coordinate system.

Now, the non-dimensional governing equations can be given in the stream- vorticity formula as follows:

$$\frac{\partial \mathcal{G}}{\partial t} + U\frac{\partial \mathcal{G}}{\partial r} + \frac{1}{r}V\frac{\partial \mathcal{G}}{\partial \theta} = Gr\left(cos(\theta)\frac{\partial T}{\partial r} - \frac{sin(\theta)}{r}\frac{\partial T}{\partial \theta}\right) + \nabla^2\mathcal{G}, \tag{33}$$

$$\frac{\partial T}{\partial T} + U\frac{\partial T}{\partial r} + \frac{1}{r}V\frac{\partial T}{\partial \theta} = \frac{1}{Pr}\nabla^2 T, \tag{34}$$

$$\mathcal{G} = -\nabla^2\psi, \tag{35}$$

$$V = -\frac{\partial \psi}{\partial r},\ U = \frac{1}{r}\frac{\partial \psi}{\partial \theta}, \tag{36}$$

where the above system is subject to the following initial and boundary conditions:

$$\mathcal{G} = \psi = T = 0 \ \text{ everywhere at } t = 0. \tag{37}$$

$$\left.\begin{array}{l} \psi = \frac{\partial \psi}{\partial r} = \frac{1}{r}\frac{\partial \psi}{\partial \theta} = 0\ ,\ \ at\ \ r = R_i\ , r = R_o, \\ T = 1\ \ at\ \ r = R_i, \\ T = 0\ \ at\ \ r = R_o\ . \end{array}\right\} \tag{38}$$

Where, $\hat{L}$ represents to the gap of annulus, R_i and R_o denotes to the ratio of inner and outer radius to the gap, respectively, Pr Prandtl number, Gr Grashof number, U, V, T, ψ and $\mathcal{G}$ refer to the radial velocity, tangent velocity, temperature, stream function and vorticity function, respectively, as well the subscripts i, o, c, h indicate to inner, outer, cold and hot, respectively.

5. Application of FT-HPM

Now, to apply the procedure of FT-HPM, first, we substituting Eq. (35) and (36) in to Eq. (33) and Eq. (34) to get the following system:

$$\frac{\partial}{\partial t}(\nabla^2\psi) + Gr\left(cos(\theta)\frac{\partial T}{\partial r} - \frac{sin(\theta)}{r}\frac{\partial T}{\partial \theta}\right) - \nabla^4\psi - \frac{1}{r}\left(\frac{\partial \psi}{\partial r}\frac{\partial}{\partial \theta}(\nabla^2\psi) - \frac{\partial \psi}{\partial \theta}\frac{\partial}{\partial r}(\nabla^2\psi)\right) = 0. \quad (39)$$

$$\frac{\partial T}{\partial T} - \frac{1}{Pr}\nabla^2 T - \frac{1}{r}\left(\frac{\partial \psi}{\partial r}\frac{\partial T}{\partial \theta} - \frac{\partial \psi}{\partial \theta}\frac{\partial T}{\partial r}\right) = 0. \quad (40)$$

Substituting $\nabla^2 = \frac{\partial^2}{\partial r^2} + \frac{1}{r}\frac{\partial}{\partial r} + \frac{1}{r^2}\frac{\partial^2}{\partial \theta^2}$ in to Eq. (39), we obtain

$$\frac{\partial}{\partial t}\left(\frac{\partial^2\psi}{\partial r^2} + \frac{1}{r}\frac{\partial \psi}{\partial r} + \frac{1}{r^2}\frac{\partial^2\psi}{\partial \theta^2}\right) + Gr\left(cos(\theta)\frac{\partial T}{\partial r} - \frac{sin(\theta)}{r}\frac{\partial T}{\partial \theta}\right) - \nabla^4\psi - \frac{1}{r}\left(\frac{\partial \psi}{\partial r}\frac{\partial(\nabla^2\psi)}{\partial \theta} - \frac{\partial \psi}{\partial \theta}\frac{\partial(\nabla^2\psi)}{\partial r}\right) = 0. \quad (41)$$

Rewriting Eq. (41) to get

$$\left[\begin{array}{c}\frac{\partial^2\psi}{\partial r \partial t} + \frac{\partial}{\partial t}\left(\frac{\partial^2\psi}{\partial r^2}r + \frac{1}{r}\frac{\partial^2\psi}{\partial \theta^2}\right) + Gr\left(rcos(\theta)\frac{\partial T}{\partial r} - sin(\theta)\frac{\partial T}{\partial \theta}\right) - r\nabla^4\psi \\ -\left(\frac{\partial \psi}{\partial r}\frac{\partial}{\partial \theta}\nabla^2\psi - \frac{\partial \psi}{\partial \theta}\frac{\partial}{\partial r}\nabla^2\psi\right)\end{array}\right] = 0. \quad (42)$$

Then, the basic steps of the new algorithm can be applied as follows:

Taking the Fourier transform with respect to r for both sides of Eq. (42), we have

$$\mathcal{F}_1\left[\frac{\partial^2\psi}{\partial r \partial t}\right] + \mathcal{F}_1\left[\begin{array}{c}\frac{\partial}{\partial t}\left(\frac{\partial^2\psi}{\partial r^2}r + \frac{1}{r}\frac{\partial^2\psi}{\partial \theta^2}\right) + Gr\left(rcos(\theta)\frac{\partial T}{\partial r} - sin(\theta)\frac{\partial T}{\partial \theta}\right) \\ -(\nabla^4\psi)r - \left(\frac{\partial \psi}{\partial r}\frac{\partial}{\partial \theta}(\nabla^2\psi) - \frac{\partial \psi}{\partial \theta}\frac{\partial}{\partial r}(\nabla^2\psi)\right)\end{array}\right] = 0. \quad (43)$$

Using the differentiation property of the Fourier transform, we obtain

$$\mathcal{F}_1\left[\frac{\partial \psi}{\partial t}\right] + \frac{1}{i\omega}\mathcal{F}_1\left[\begin{array}{c}\frac{\partial}{\partial t}\left(\frac{\partial^2\psi}{\partial r^2}r + \frac{1}{r}\frac{\partial^2\psi}{\partial \theta^2}\right) + Gr\left(rcos(\theta)\frac{\partial T}{\partial r} - sin(\theta)\frac{\partial T}{\partial \theta}\right) \\ -(\nabla^4\psi)r - \left(\frac{\partial \psi}{\partial r}\frac{\partial}{\partial \theta}(\nabla^2\psi) - \frac{\partial \psi}{\partial \theta}\frac{\partial}{\partial r}(\nabla^2\psi)\right)\end{array}\right] = 0. \quad (44)$$

Taking the inverse FT for both sides of Eq. (44), we get:

$$\frac{\partial\psi}{\partial t}+\mathcal{F}_1^{-1}\left[\frac{1}{i\omega}\mathcal{F}_1\left\{\begin{matrix}\frac{\partial}{\partial t}\left(\frac{\partial^2\psi}{\partial r^2}r+\frac{1}{r}\frac{\partial^2\psi}{\partial\theta^2}\right)+Gr\left(rcos(\theta)\frac{\partial T}{\partial r}-sin(\theta)\frac{\partial T}{\partial\theta}\right)\\ -(\nabla^4\psi)r-\left(\frac{\partial\psi}{\partial r}\frac{\partial}{\partial\theta}(\nabla^2\psi)-\frac{\partial\psi}{\partial\theta}\frac{\partial}{\partial r}(\nabla^2\psi)\right)\end{matrix}\right\}\right]=0. \quad (45)$$

Now, we using the HPM idea on Eq. (40) and (45), we have

$$(1-p)\left[\frac{\partial\psi}{\partial t}-\psi_0^*\right]+p\left[\begin{matrix}\frac{\partial\psi}{\partial t}+\\ \mathcal{F}_1^{-1}\left(\frac{1}{i\omega}\mathcal{F}_1\left[\begin{matrix}\frac{\partial}{\partial t}\left(\frac{\partial^2\psi}{\partial r^2}r+\frac{1}{r}\frac{\partial^2\psi}{\partial\theta^2}\right)+Gr\left(\begin{matrix}rcos(\theta)\frac{\partial T}{\partial r}\\ -sin(\theta)\frac{\partial T}{\partial\theta}\end{matrix}\right)\\ -(\nabla^4\psi)r-\left(\frac{\partial\psi}{\partial r}\frac{\partial}{\partial\theta}(\nabla^2\psi)-\frac{\partial\psi}{\partial\theta}\frac{\partial}{\partial r}(\nabla^2\psi)\right)\end{matrix}\right]\right)\end{matrix}\right]=0. \quad (46)$$

$$(1-p)\left[\frac{\partial T}{\partial t}-T_0^*\right]+p\left[\frac{\partial T}{\partial t}-\frac{1}{Pr}\nabla^2T-\frac{1}{r}\left(\frac{\partial\psi}{\partial r}\frac{\partial T}{\partial\theta}-\frac{\partial\psi}{\partial\theta}\frac{\partial T}{\partial r}\right)\right]=0. \quad (47)$$

The rearrangement of the above system leads to

$$\frac{\partial\psi}{\partial t}-\psi_0^*+p\psi_0^*+p\mathcal{F}_1^{-1}\left[\frac{1}{i\omega}\mathcal{F}_1\left\{\begin{matrix}\frac{\partial}{\partial t}\left(\frac{\partial^2\psi}{\partial r^2}r+\frac{1}{r}\frac{\partial^2\psi}{\partial\theta^2}\right)+Gr\left(rcos(\theta)\frac{\partial T}{\partial r}-sin(\theta)\frac{\partial T}{\partial\theta}\right)\\ -(\nabla^4\psi)r-\left(\frac{\partial\psi}{\partial r}\frac{\partial}{\partial\theta}(\nabla^2\psi)-\frac{\partial\psi}{\partial\theta}\frac{\partial}{\partial r}(\nabla^2\psi)\right)\end{matrix}\right\}\right]=0. \quad (48)$$

$$\frac{\partial T}{\partial t}-T_0^*+pT_0^*-p\left[\frac{1}{Pr}\nabla^2T+\frac{1}{r}\left(\frac{\partial\psi}{\partial r}\frac{\partial T}{\partial\theta}-\frac{\partial\psi}{\partial\theta}\frac{\partial T}{\partial r}\right)\right]=0. \quad (49)$$

by applying the Fourier transform with respect to t on both sides of Eq. (48) and (49), we have

$$\mathcal{F}_2[\psi]=\frac{1}{i\omega}\mathcal{F}_2[\psi_0^*]-\frac{1}{i\omega}\mathcal{F}_2\left\{p\psi_0^*+p\mathcal{F}_1^{-1}\left[\frac{1}{i\omega}\mathcal{F}_1\left\{\begin{matrix}\frac{\partial}{\partial t}\left(\frac{\partial^2\psi}{\partial r^2}\right)r+\frac{1}{r}\frac{\partial}{\partial t}\left(\frac{\partial^2\psi}{\partial\theta^2}\right)-(\nabla^4\psi)r\\ +Gr\left(rcos(\theta)\frac{\partial T}{\partial r}-sin(\theta)\frac{\partial T}{\partial\theta}\right)\\ -\left(\frac{\partial\psi}{\partial r}\frac{\partial}{\partial\theta}(\nabla^2\psi)-\frac{\partial\psi}{\partial\theta}\frac{\partial}{\partial r}(\nabla^2\psi)\right)\end{matrix}\right\}\right]\right\}. \quad (50)$$

$$\mathcal{F}_2[T]=\frac{1}{i\omega}\mathcal{F}_2[T_0^*]-\frac{1}{i\omega}\mathcal{F}_2\left[pT_0^*-p\left\{\frac{1}{Pr}\nabla^2T+\frac{1}{r}\left(\frac{\partial\psi}{\partial r}\frac{\partial T}{\partial\theta}-\frac{\partial\psi}{\partial\theta}\frac{\partial T}{\partial r}\right)\right\}\right]. \quad (51)$$

Taking the inverse FT for both sides of Eq. (50) and (51), we deduce

$$\psi=\mathcal{F}_2^{-1}\left[\frac{1}{i\omega}\mathcal{F}_2[\psi_0^*]-\frac{1}{i\omega}\mathcal{F}_2\left\{p\psi_0^*+p\mathcal{F}_1^{-1}\left[\frac{1}{i\omega}\mathcal{F}_1\left\{\begin{matrix}\frac{\partial}{\partial t}\left(\frac{\partial^2\psi}{\partial r^2}\right)r+\frac{1}{r}\frac{\partial}{\partial t}\left(\frac{\partial^2\psi}{\partial\theta^2}\right)-(\nabla^4\psi)r\\ +Gr\left(rcos(\theta)\frac{\partial T}{\partial r}-sin(\theta)\frac{\partial T}{\partial\theta}\right)\\ -\left(\frac{\partial\psi}{\partial r}\frac{\partial}{\partial\theta}(\nabla^2\psi)-\frac{\partial\psi}{\partial\theta}\frac{\partial}{\partial r}(\nabla^2\psi)\right)\end{matrix}\right\}\right]\right\}\right]. \quad (52)$$

$$T=\mathcal{F}_2^{-1}\left[\frac{1}{i\omega}\mathcal{F}_2[T_0^*]-\frac{1}{i\omega}\mathcal{F}_2\left\{pT_0^*-p\left[\frac{1}{Pr}\nabla^2T+\frac{1}{r}\left(\frac{\partial\psi}{\partial r}\frac{\partial T}{\partial\theta}-\frac{\partial\psi}{\partial\theta}\frac{\partial T}{\partial r}\right)\right]\right\}\right]. \quad (53)$$

From the assumption of the HPM, we have

$$\psi = \sum_{j=0}^{\infty} p^j \psi_j \text{ and } T = \sum_{j=0}^{\infty} p^j T_j. \tag{54}$$

and the nonlinear terms can be represented as:

$$\frac{\partial \psi}{\partial \theta}\frac{\partial \nabla^2 \psi}{\partial r} = \sum_{j=0}^{\infty} p^j H_j \text{ , } \frac{\partial \psi}{\partial r}\frac{\partial \nabla^2 \psi}{\partial \theta} = \sum_{j=0}^{\infty} p^j H_j^*, \frac{\partial \psi}{\partial \theta}\frac{\partial T}{\partial r} = \sum_{j=0}^{\infty} p^j G_j \text{ and } \frac{\partial \psi}{\partial r}\frac{\partial T}{\partial \theta} = \sum_{j=0}^{\infty} p^j G_j^* \tag{55}$$

Substituting Eq_s. (54) and (55) in to Eq_s. (52) and (53), we get

$$\sum_{j=0}^{\infty} p^j \psi_j = \mathcal{F}_2^{-1}\left[\begin{array}{c} \frac{1}{i\omega}\mathcal{F}_2[\psi_0^*] - \frac{p}{i\omega}\mathcal{F}_2[\psi_0^*] - \\ \frac{p}{i\omega}\mathcal{F}_2\left\{\mathcal{F}_1^{-1}\left[\frac{1}{i\omega}\mathcal{F}_1\left\{\begin{array}{l} \frac{\partial}{\partial t}\left(\frac{\partial^2}{\partial r^2}\sum_{j=0}^{\infty} p^j\psi_j\right)r + \frac{1}{r}\frac{\partial}{\partial t}\left(\frac{\partial^2}{\partial \theta^2}\sum_{j=0}^{\infty} p^j\psi_j\right) + \\ Gr\left(rcos(\theta)\frac{\partial \sum_{j=0}^{\infty} p^j T_j}{\partial r} - sin(\theta)\frac{\partial \sum_{j=0}^{\infty} p^j T_j}{\partial \theta}\right) - \\ \left(\nabla^4 \sum_{j=0}^{\infty} p^j\psi_j\right)r - \left(\sum_{j=0}^{\infty} p^j H_j^* - \sum_{j=0}^{\infty} p^j H_j\right) \end{array}\right\}\right]\right\} \end{array}\right]. \tag{56}$$

$$\sum_{j=0}^{\infty} p^j T_j = \mathcal{F}_2^{-1}\left[\frac{1}{i\omega}\mathcal{F}_2[T_0^*] - \frac{p}{i\omega}\mathcal{F}_2[T_0^*] + \frac{p}{i\omega}\mathcal{F}_2\left\{\begin{array}{l} \frac{1}{Pr}\nabla^2\sum_{j=0}^{\infty} p^j T_j + \\ \frac{1}{r}\left(\sum_{j=0}^{\infty} p^j G_j^* - \sum_{j=0}^{\infty} p^j G_j\right) \end{array}\right\}\right]. \tag{57}$$

Comparing the coefficients of the same powers of p, we obtain

$$p^0: \begin{cases} \psi_0 = \mathcal{F}_2^{-1}\left[\frac{1}{i\omega}\mathcal{F}_2[\psi_0^*]\right] \\ T_0 = \mathcal{F}_2^{-1}\left[\frac{1}{i\omega}\mathcal{F}_2[T_0^*]\right] \end{cases}, \tag{58}$$

$$p^1: \begin{cases} \psi_1 = \mathcal{F}_2^{-1}\left[\begin{array}{c} \frac{-1}{i\omega}\mathcal{F}_2[\psi_0^*] - \\ \frac{1}{i\omega}\mathcal{F}_2\left\{\mathcal{F}_1^{-1}\left[\frac{1}{i\omega}\mathcal{F}_1\left\{\begin{array}{l} \frac{\partial}{\partial t}\left(\frac{\partial^2\psi_0}{\partial r^2}\right)r + \frac{1}{r}\frac{\partial}{\partial t}\left(\frac{\partial^2\psi_0}{\partial \theta^2}\right) - (H_0^* - H_0) - \\ (\nabla^4\psi_0)r + Gr\left(rcos(\theta)\frac{\partial T_0}{\partial r} - sin(\theta)\frac{\partial T_0}{\partial \theta}\right) \end{array}\right\}\right]\right\} \end{array}\right] \\ T_1 = \mathcal{F}_2^{-1}\left[\frac{-1}{i\omega}\mathcal{F}_2[T_0^*] + \frac{1}{i\omega}\mathcal{F}_2\left\{\frac{1}{Pr}\nabla^2 T_0 + \frac{1}{r}(G_0^* - G_0)\right\}\right] \end{cases}, \tag{59}$$

$$p^2: \begin{cases} \psi_2 = \mathcal{F}_2^{-1}\left[\frac{-1}{i\omega}\mathcal{F}_2\left\{\mathcal{F}_1^{-1}\left[\frac{1}{i\omega}\mathcal{F}_1\left\{\begin{array}{l} \frac{\partial}{\partial t}\left(\frac{\partial^2\psi_1}{\partial r^2}\right)r + \frac{1}{r}\frac{\partial}{\partial t}\left(\frac{\partial^2\psi_1}{\partial \theta^2}\right) - (H_1^* - H_1) - \\ (\nabla^4\psi_1)r + Gr\left(rcos(\theta)\frac{\partial T_1}{\partial r} - sin(\theta)\frac{\partial T_1}{\partial \theta}\right) \end{array}\right\}\right]\right\}\right] \\ T_2 = \mathcal{F}_2^{-1}\left[\frac{1}{i\omega}\mathcal{F}_2\left\{\frac{1}{Pr}\nabla^2 T_1 + \frac{1}{r}(G_1^* - G_1)\right\}\right] \end{cases}, \tag{60}$$

$$\vdots$$

$$p^j: \begin{cases} \psi_j = \mathcal{F}_2^{-1}\left[\frac{-1}{i\omega}\mathcal{F}_2\left\{\mathcal{F}_1^{-1}\left[\frac{1}{i\omega}\mathcal{F}_1\left\{\begin{array}{l} \frac{\partial}{\partial t}\left(\frac{\partial^2\psi_{j-1}}{\partial r^2}\right)r + \frac{1}{r}\frac{\partial}{\partial t}\left(\frac{\partial^2\psi_{j-1}}{\partial \theta^2}\right) - \left(H_{j-1}^* - H_{j-1}\right) - \\ (\nabla^4\psi_{j-1})r + Gr\left(rcos(\theta)\frac{\partial T_{j-1}}{\partial r} - sin(\theta)\frac{\partial T_{j-1}}{\partial \theta}\right) \end{array}\right\}\right]\right\}\right] \\ T_j = \mathcal{F}_2^{-1}\left[\frac{1}{i\omega}\mathcal{F}_2\left\{\frac{1}{Pr}\nabla^2 T_{j-1} + \frac{1}{r}\left(G_{j-1}^* - G_{j-1}\right)\right\}\right] \end{cases}. \tag{61}$$

Where,

$$H_0 = \frac{\partial\psi_0}{\partial\theta}\frac{\partial\nabla^2\psi_0}{\partial r},\ H_0^* = \frac{\partial\psi_0}{\partial r}\frac{\partial\nabla^2\psi_0}{\partial\theta},\ H_1 = \frac{\partial\psi_0}{\partial\theta}\frac{\partial\nabla^2\psi_1}{\partial r} + \frac{\partial\psi_1}{\partial\theta}\frac{\partial\nabla^2\psi_0}{\partial r} \text{ and } H_1^* = \frac{\partial\psi_0}{\partial r}\frac{\partial\nabla^2\psi_1}{\partial\theta} + \frac{\partial\psi_1}{\partial r}\frac{\partial\nabla^2\psi_0}{\partial\theta}.$$

$$G_0 = \frac{\partial\psi_0}{\partial\theta}\frac{\partial T_0}{\partial r},\ G_0^* = \frac{\partial\psi_0}{\partial r}\frac{\partial T_0}{\partial\theta},\ G_1 = \frac{\partial\psi_0}{\partial\theta}\frac{\partial T_1}{\partial r} + \frac{\partial\psi_1}{\partial\theta}\frac{\partial T_0}{\partial r} \text{ and } G_1^* = \frac{\partial\psi_0}{\partial r}\frac{\partial T_1}{\partial\theta} + \frac{\partial\psi_1}{\partial r}\frac{\partial T_0}{\partial\theta}. \quad (62)$$

In the porous annulus, the field of flow can be segmented into three regions: an inner boundary layer located near the inner cylinder, an outer boundary layer located near the outer cylinder, and a core region located between the two layers. Using the initial solutions which found by Pop et al. [12] in addition to the initial and boundary conditions in equations (37) and (38), the solution of equation (58) in the three regions can be given as follows:

$$\psi_0^i = 2\sqrt{t}\,T_i\left(-\eta\,erfc(\eta) + \frac{1}{\sqrt{\pi}}\left(e^{-\eta^2}-1\right)\right)sin(\theta)\ ,\ T_0^i = T_i erfc(\eta), \quad (63)$$

$$\psi_0^o = 2\sqrt{t}\,T_o\left(\xi\,erfc(\xi) - \frac{1}{\sqrt{\pi}}\left(e^{-\xi^2}-1\right)\right)sin(\theta)\ ,\ T_0^o = T_o erfc(\xi), \quad (64)$$

$$\psi_0^c = \frac{2\sqrt{t}}{\sqrt{\pi}(R^2-1)}\left((T_i + R\,T_o)r - (T_o + R\,T_i)r^{-1}\right)sin(\theta)\ ,\ T_0^c = 0. \quad (65)$$

And then, the solutions of Eq. (59) are given in the following forms:

$$\psi_1^i = \frac{cos(\theta)}{\sqrt{t}\pi^{3/2}r^2}\begin{bmatrix} T_i\left(\pi T_i\left\{(ln(r)\,r^2 + 6rt - 4t)\,erfc(\eta) - 8T_i t^{\frac{3}{2}}\sqrt{\pi} + 2T_i t^{\frac{3}{2}}\sqrt{\pi}\right\}sin(\theta)\right)e^{-\eta^2} \\ +\cdots + Grr^2 t\,cos(\theta) \\ -2\left(\begin{matrix}\left\{\sqrt{\pi}T_i\left(\sqrt{t}r^2 l\,n(r) - 2t^{\frac{3}{2}}\right)e^{-\eta^2} + \frac{3}{2}\left(r-\frac{1}{3}\right)\sqrt{t}\pi^{\frac{3}{2}}erfc^2(\eta)\right\}T_i + \\ \left(\pi^{3/2}\left(\frac{3}{4}t^{\frac{3}{2}} + T_i\sqrt{t}(1-3r)\right) + 3T_i\pi\left(r-\frac{2}{3}\right)\right)erfc(\eta) + \cdots\end{matrix}\right)sin(\theta)\end{bmatrix}, \quad (66)$$

$$T_1^i = \frac{-T_i\,e^{-\eta^2}}{\sqrt{t}\pi^{3/2}rPr}\begin{bmatrix} -4\sqrt{\pi}PrT_i t^{\frac{3}{2}}e^{-\eta^2}\,cos(\theta) - 4\pi PrT_i t(r-1)erfc(\eta)\,cos(\theta) \\ +\,4\,\sqrt{\pi}PrT_i\,t^{\frac{3}{2}}cos(\theta) + 4\,\pi\,t\,PrT_i(r-1)\,cos(\theta) + \\ \pi(Pr(r^2-r) - r^2 + r + 4t)\end{bmatrix}, \quad (67)$$

$$\psi_1^o = \frac{sin(\theta)}{\sqrt{t}\pi^{3/2}r^2}\begin{bmatrix} \pi T_o^2 \begin{Bmatrix} \left(\frac{r^5}{3} + R^2r^3 - Rr^4 + \frac{8}{3}Rr^2 - \right) erfc(\xi) - \\ 4Rt^2 - 2R\,ln(r)\,tr^2 \end{Bmatrix} cos(\theta)\, e^{-\xi^2} \\ + \begin{Bmatrix} -\sqrt{\pi}T_O \left(2\,ln(r)\,t^{\frac{3}{2}}r^2 - 2t^{\frac{5}{2}} + ln(t)\sqrt{t}\left(Rr^3 - \frac{r^4}{2}\right)\right) e^{-\xi^2} \\ + \cdots \end{Bmatrix} cos(\theta) \\ + \cdots + \frac{8}{3}t\pi\left(\left(R - \frac{3}{2}r\right)cos(\theta) + \frac{3}{4}ln(r)\,r^2 - \frac{3}{4}r^2 + \frac{3}{4}t\right) \end{bmatrix}, \quad (68)$$

$$T_1^o = \frac{T_o\, e^{-\xi^2}}{\sqrt{t}\pi^{3/2}rPr}\begin{bmatrix} \sqrt{\pi}PrT_o t^{\frac{3}{2}} e^{-\xi^2}\, cos(\theta) + \pi PrT_o t(R-r)erfc(\xi)\, cos(\theta) - \\ \pi\left(tPrT_o(R-r)\,cos(\theta) + \frac{1}{4}Pr(R-r)r - \frac{1}{4}Rr + \frac{1}{4}r^2 - t\right), \\ -\sqrt{\pi}PrT_o t^{\frac{3}{2}}\, cos(\theta) \end{bmatrix}, \quad (69)$$

$$\psi_1^c = 0\ ,\ T_1^c = 0. \quad (70)$$

$\vdots$

Where, $\eta = \frac{r-1}{2\sqrt{t}}$, $\xi = \frac{R-r}{2\sqrt{t}}$, T_i and T_o refer to the inner and outer cylinder temperatures, respectively, R denotes to the radius ratio.

Then the analytical approximate solutions ψ and T can be given by setting $p = 1$ as:

$$\psi = \lim_{N\to\infty}\left(\sum_{j=0}^{N}\psi_j^i + \sum_{j=0}^{N}\psi_j^o + \sum_{j=0}^{N}\psi_j^c\right). \quad (71)$$

$$T = \lim_{N\to\infty}\left(\sum_{j=0}^{N}T_j^i + \sum_{j=0}^{N}T_j^o + \sum_{j=0}^{N}T_j^c\right). \quad (72)$$

6. Results and Discussion

This discusses the effect of Grashof number and the diameter ratio on the analytical results of the problem two-dimensional transient natural convection in a horizontal cylindrical concentric annulus bounded by two isothermal surfaces which obtained by applying the new technique (FT-HPM).

6.1. Streamline and Isotherm patterns

To illustrate the heat transfer within the cylinders, the streamlines and isotherm contours are used. Figs. (2) and (3) compare the results of the current work with those of previous works [2, 7, 17] at $R = 2$, $Pr = 0.71$ and for Grashof number values of 10000 and 38800, respectively. In these figures, we notice a good agreement of the analytical results of the current method with the results

of the mentioned studies and at the same values of the Grashof and Prandtl numbers and the ratio of the radius.

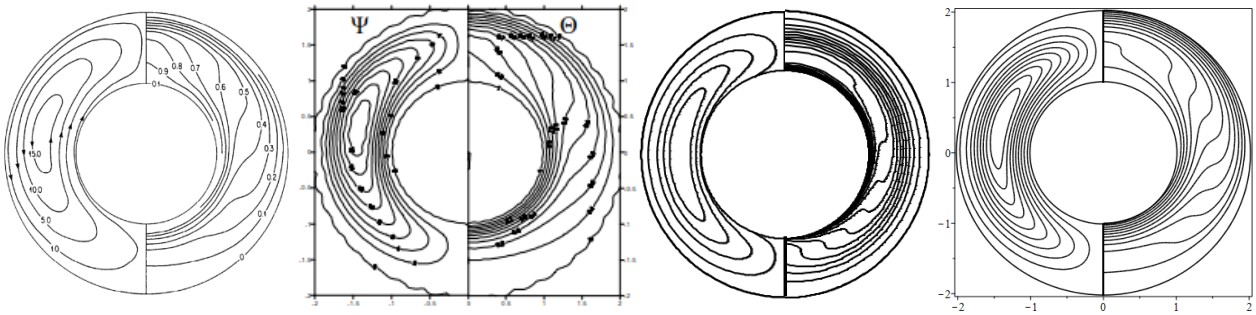

(**a**) (**b**) (**c**) (**d**)

Figure 2: Comparison of results between (a) [17], (b) [7], (c) [2] and (d) FLT-HPM for stream (left) and isotherm (right) for $\mathrm{Gr} = 10000$, $\mathrm{Pr} = 0.71$ and $\mathrm{R} = 2$.

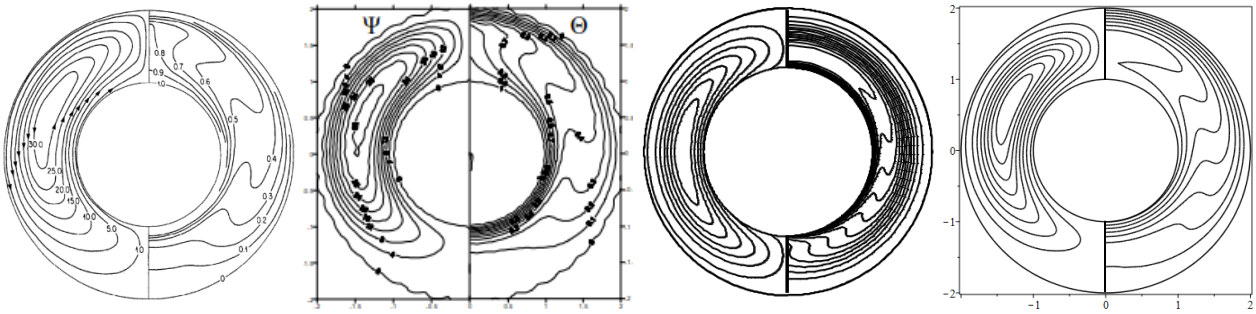

(**a**) (**b**) (**c**) (**d**)

Figure 3: Comparison of results between (a) [17], (b) [7], (c) [2] and (d) FLT-HPM for stream (left) and isotherm (right) for $Gr = 38800$, $Pr = 0.71$ and $R = 2$.

In Fig. (4-a, b, c), the Grashof number of the range $(10^3 \leq Gr \leq 4 \times 10^4)$ as well as different radius ratios ($R = 1.2$, 1.5 and 2.0) at Prandtl number of 0.7 are considered.

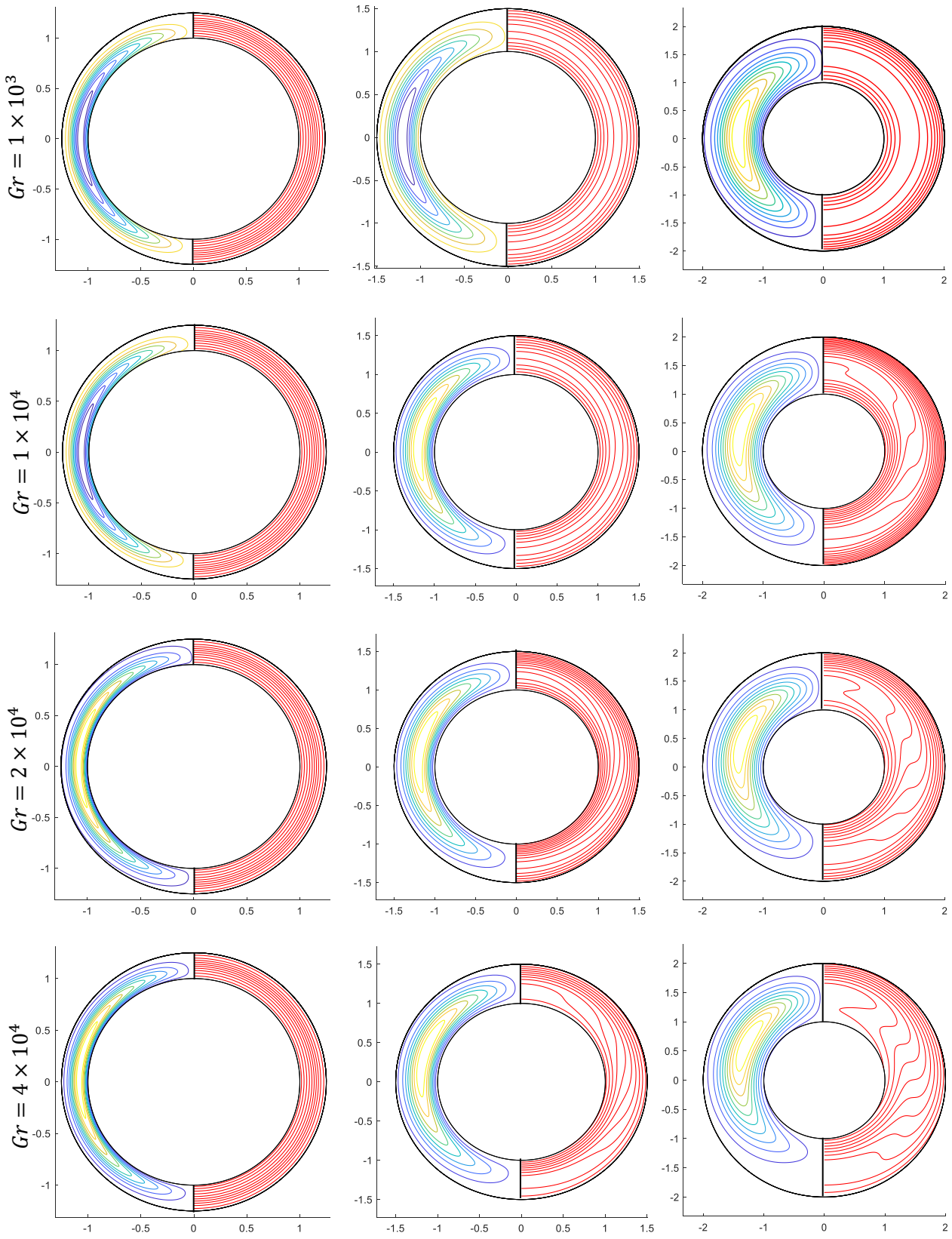

(a) $R = 1.2$ **(b)** $R = 1.5$ **(c)** $R = 2$

Figure 4: Streamline (left) and Isotherms (right) at Different Grashof number, Pr =

Figure 4a shows that there is no obvious change in the flow pattern and temperature fields at $R = 1.2$ with different values of Grashof number. In this case, the temperature pattern is similar to circles when the radius ratio is small, and this indicates the weak effect of thermal currents. With the increase of the radius ratio to 1.5, Fig. (4-b) shows that the flow pattern starts with an upward displacement, in addition, the temperature pattern remains similar to circles when Grashof number lies between 10^3 and 10^4, and begins to deform slightly when the Grashof number increases to 4×10^4 and this indicates an effect of convective currents. Figure (4-c) illustrates that there is an obvious change in the flow pattern and temperature domains at $R = 2$ with different values of the Grashof number. In this case, the flux gap moves upwards significantly, in addition, the distortion of the temperature pattern increases with increasing Grashof number up to 4×10^4 and this indicates an increase in the heat convection. In order to show the efficiency and accuracy of the suggested method (FT-HPM) in finding approximate analytical solutions to the current problem, we have to present the following two Tables:

Table 1: Comparison the absolute error of FT-HPM with YT-HPM [2] and HPM [2] of $\psi(r,\theta)$ at $Gr = 1000$, $Pr = 0.7$ and $R = 2$.

θ	r	$t = 0.01$			$t = 0.1$		
		FT-HPM	YT-HPM [2]	HPM [2]	FT-HPM	YT-HPM [2]	HPM [2]
0	1	1.88×10^{-7}	2.82×10^{-1}	56.983	0.16×10^{-3}	8.921	196.254
	1.5	2.99×10^{-8}	5.44×10^{-4}	1.10×10^{-1}	0.22×10^{-3}	4.775	105.047
	2	1.11×10^{-12}	3.91×10^{-12}	7.91×10^{-10}	0.13×10^{-3}	7.32×10^{-1}	16.109
30	1	2.83×10^{-9}	5.85×10^{-2}	11.811	0.24×10^{-4}	1.463	32.164
	1.5	4.66×10^{-9}	2.09×10^{-4}	4.23×10^{-2}	0.34×10^{-4}	7.54×10^{-1}	16.574
	2	1.38×10^{-9}	1.02×10^{-6}	2.08×10^{-4}	0.20×10^{-4}	1.03×10^{-1}	2.254
60	1	1.79×10^{-8}	2.64×10^{-1}	53.355	0.15×10^{-3}	8.472	186.363
	1.5	2.85×10^{-8}	6.10×10^{-4}	1.23×10^{-1}	0.21×10^{-3}	4.544	99.954
	2	1.05×10^{-8}	3.69×10^{-7}	6.98×10^{-5}	0.12×10^{-3}	7.01×10^{-1}	15.419
90	1	8.38×10^{-9}	1.39×10^{-1}	28.240	0.72×10^{-4}	4.071	89.597
	1.5	1.34×10^{-8}	2.30×10^{-5}	4.55×10^{-3}	0.99×10^{-4}	2.152	47.371
	2	5.09×10^{-9}	1.01×10^{-6}	1.97×10^{-4}	0.58×10^{-4}	1.18×10^{-1}	7.001
180	1	1.13×10^{-8}	1.65×10^{-1}	31.681	0.97×10^{-4}	5.274	115.973
	1.5	1.79×10^{-8}	6.65×10^{-4}	1.14×10^{-1}	0.13×10^{-3}	2.847	62.603
	2	6.56×10^{-9}	9.24×10^{-7}	1.79×10^{-4}	0.77×10^{-4}	4.48×10^{-1}	9.837

Table 2: Comparison the absolute error of FT-HPM with YT-HPM [2] and HPM [2] of $T(r,\theta)$ at $Gr = 1000$, $Pr = 0.7$ and $R = 2$.

θ	r	$t = 0.01$			$t = 0.1$		
		FT-HPM	YT-HPM [2]	HPM [2]	FT-HPM	YT-HPM [2]	HPM [2]
0	1	2.08×10^{-7}	3.25×10^{-3}	17.571	0.23×10^{-5}	3.23×10^{-2}	3.635
	1.5	6.1×10^{-10}	2.59×10^{-5}	3.38×10^{-3}	0.24×10^{-5}	2.76×10^{-2}	5×10^{-1}
	2	5.9×10^{-14}	3.7×10^{-13}	5.59×10^{-11}	0.25×10^{-5}	7.01×10^{-3}	8×10^{-2}
30	1	9.2×10^{-15}	1.81×10^{-2}	318.479	0.12×10^{-4}	1.586	380.42
	1.5	2.2×10^{-8}	2.58×10^{-5}	2.95×10^{-3}	0.34×10^{-5}	2.81×10^{-1}	72.411
	2	2.9×10^{-13}	3.7×10^{-13}	5.59×10^{-11}	0.73×10^{-5}	1.55×10^{-3}	1.183
60	1	2.0×10^{-8}	3.48×10^{-3}	115.391	0.46×10^{-5}	4.85×10^{-1}	121.08
	1.5	7.5×10^{-9}	2.59×10^{-5}	3.99×10^{-3}	0.48×10^{-5}	6.78×10^{-2}	22.35
	2	1.7×10^{-13}	3.7×10^{-13}	5.59×10^{-11}	0.50×10^{-5}	5.51×10^{-3}	2×10^{-1}
90	1	2.0×10^{-7}	1.22×10^{-2}	282.258	0.10×10^{-4}	1.405	342.26
	1.5	3.0×10^{-8}	5.59×10^{-5}	4.74×10^{-3}	0.27×10^{-5}	2.91×10^{-1}	65.903
	2	1.1×10^{-13}	3.7×10^{-13}	5.95×10^{-11}	0.58×10^{-5}	1.17×10^{-2}	1.271
180	1	4.6×10^{-12}	1.40×10^{-2}	270.701	0.25×10^{-4}	1.289	311.13
	1.5	3.7×10^{-8}	2.59×10^{-5}	3.44×10^{-3}	0.69×10^{-5}	2.22×10^{-1}	58.82
	2	2.3×10^{-13}	3.7×10^{-13}	5.59×10^{-11}	0.14×10^{-4}	2.69×10^{-3}	9×10^{-1}

From the comparison of the absolute errors of the approximate solutions of the studied problem and as shown in Tables (1) and (2) the absolute errors in the results of the proposed method (FT-HPM) are less than the absolute errors of the results previously calculated using YT-HPM and HPM at $Gr = 1000$ and $Pr = 0.7$, so we can say that the new method has higher accuracy and efficiency than the mentioned methods [2].

6.2. Velocity distribution

To study the velocity distribution, we use the velocity component in the θ-direction (The tangent velocity), which can be calculated by differentiating Eq. (71) with respect to r. Fig. (5-a, b, c) shows the velocity diagram for $Gr = 1000$, $Pr = 0.71$, $t = 0.01$ with different values of radius ratios ($R = 1.2, 1.5, 2$) and $\theta = n(30°)$, $1 < n < 5$.

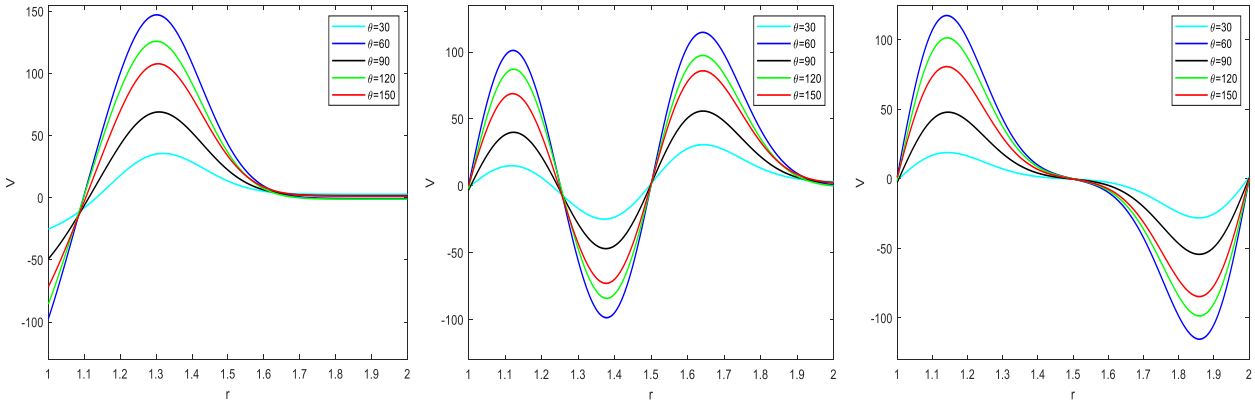

(***a***) (***b***) (***c***)

Figure 5: θ-component of velocity versus radial position at θ = n(30°), 1 < n < 5, for Gr = 1000, Pr = 0.71, t = 0.01 and (a) R = 1.2, (b) R = 1.5 , (c) R =

It is clear from Fig. 5 and for all cases (a, b, c) the effect of the radius ratio on the velocity level. It was noted that the absolute maximum values of velocity are in the following order, largest for $\theta = 60°$, next largest for 120°, followed by 150°, 90°, and the minimum value of the velocity is at $\theta = 30°$.

6.3 Heat transfer rates

The local Nusselt numbers $Nu_i(\theta)$ and $Nu_o(\theta)$ are used to express the local heat flow rates per unit area in the inner and outer cylinders, respectively. In the same way, the means of the overall Nusselt number $\overline{Nu}$ is used to express the total heat flow rate from the inner cylinder to the outer cylinder. Moreover, the local Nusselt numbers $Nu_i(\theta)$ and $Nu_o(\theta)$, and the mean Nusselt number $\overline{Nu}$ are defined respectively as follows:

$$Nu_i = -ln(R)\left[r\frac{\partial T}{\partial r}\right]_{r=R_i}, \tag{73-a}$$

$$Nu_o = -ln(R)\left[r\frac{\partial T}{\partial r}\right]_{r=R_o}, \tag{73-b}$$

$$\overline{Nu_i} = -\frac{ln(R)}{\pi}\int_0^{\pi}\left[r\frac{\partial T}{\partial r}\right]_{r=R_i} d\theta, \tag{73-c}$$

$$\overline{Nu_o} = -\frac{ln(R)}{\pi}\int_0^{\pi}\left[r\frac{\partial T}{\partial r}\right]_{r=R_o} d\theta. \tag{73-d}$$

Both mean Nusselt numbers ($\overline{Nu_i}$, $\overline{Nu_o}$) vs. the non-dimensional time t are plotted in Figs. (6-12) at $Pr = 0.7$ with different values for both Grashof number and radius ratios. Figs. (6), (7) and (8) show the mean Nusselt numbers ($\overline{Nu_i}$, $\overline{Nu_o}$) at $R = 1.5$ with $Gr = 4850$, $Gr = 11500$ and $Gr = 26200$, respectively. It is clear from this figures that when the Grashof number increases, the mean of the Nusselt numbers ($\overline{Nu_i}$, $\overline{Nu_o}$) increases at the radius ratio of 1.5. In addition, Figs. (9), (10) and (11) illustrate the mean Nusselt numbers ($\overline{Nu_i}$, $\overline{Nu_o}$) at $R = 2$ with $Gr = 1000$, $Gr = 38800$ and $Gr = 88000$, respectively. It is seen from these figures that the mean Nusselt number increases when the Grashof number increases at a radius ratio of 2. In the above cases and for all Figs. (6-11) we note that when t increases, the mean of Nusselt numbers ($\overline{Nu_i}$, $\overline{Nu_o}$) comes close to their steady-state values. Furthermore, Fig. 12 exhibits the mean Nusselt numbers ($\overline{Nu_i}$, $\overline{Nu_o}$) at $Gr = 732$ and $R = 1.2$. this figure show that the mean Nusselt numbers ($\overline{Nu_i}$, $\overline{Nu_o}$) approach unity at t increases. This indicates that convection is almost non-existent at the stated values.

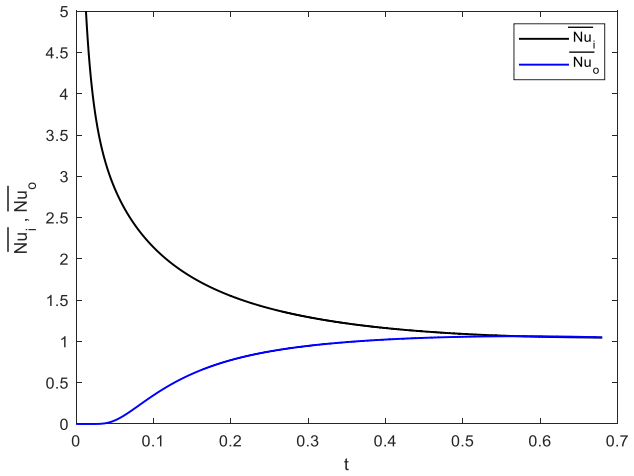

Figure 6: Mean Nusselt number for Gr = 4850, Pr = 0.7, and R = 1.5.

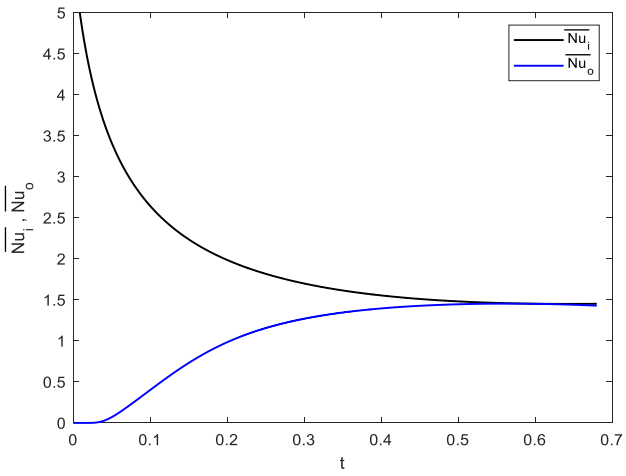

Figure 7: Mean Nusselt number for Gr = 11500, Pr = 0.7, and R = 1.5.

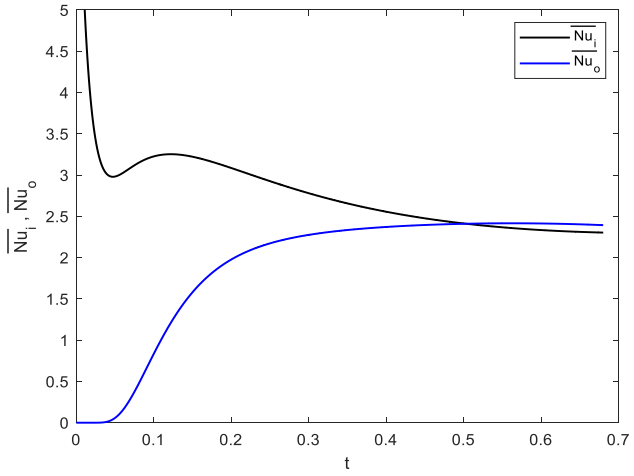

Figure 8: *Mean Nusselt number for* $Gr = 26200$, $Pr = 0.7$, and $R = 1.5$.

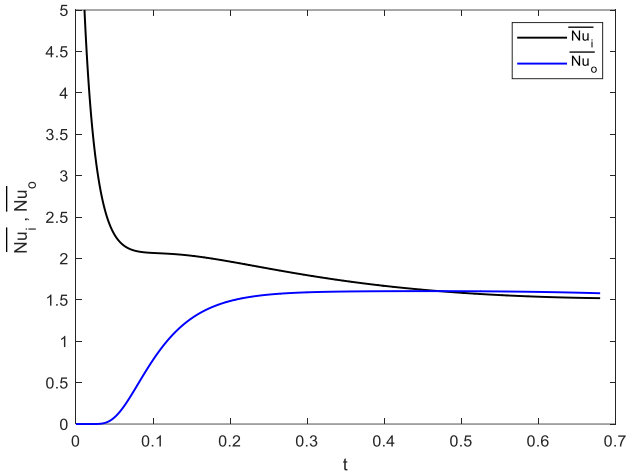

Figure 9: *Mean Nusselt number for* $Gr = 10000$, $Pr = 0.7$, and $R = 2$.

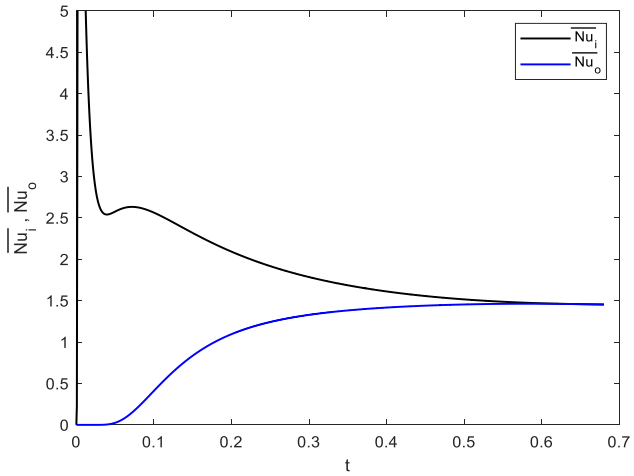

Figure 10: *Mean Nusselt number for* $Gr = 38800$, $Pr = 0.7$, and $R = 2$.

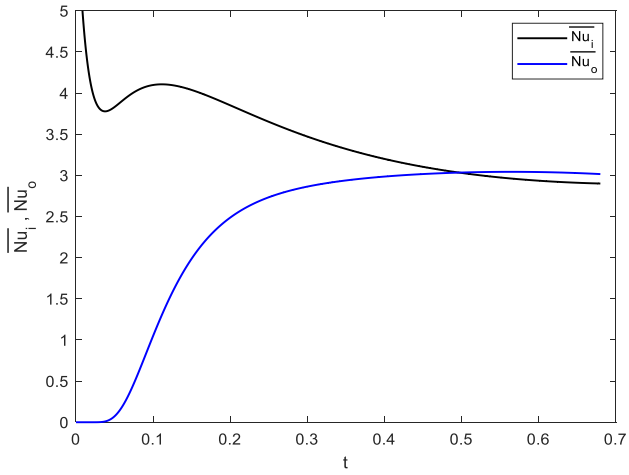

Figure 11: *Mean Nusselt number for* $Gr = 88000$, $Pr = 0.7$, and $R = 2$.

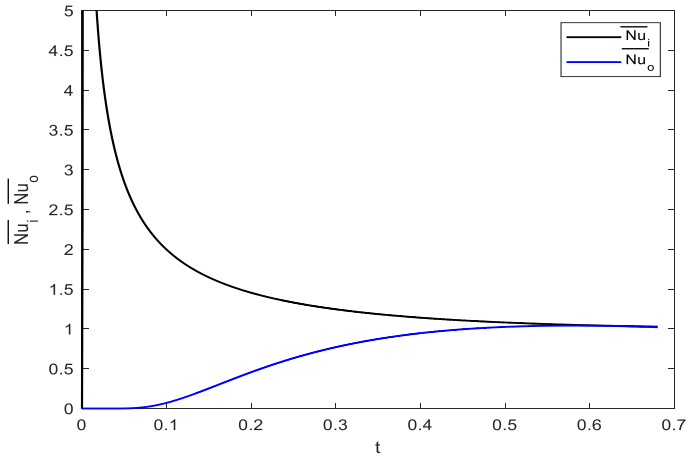

Figure 12: *Mean Nusselt number for* $Gr = 732$, $Pr = 0.7$, and $R = 1.2$.

Table 3: Comparison of the mean Nusselt number with [17] and [7] at $Pr = 0.7$ with various values of Gr

R	Gr	Mean Nusselt Number ($\overline{Nu}$)		
		FT-HPM	[18]	[7]
2	10000	1.69	1.64	1.658
	38800	2.20	2.4	2.42
	88000	3.05	3.08	2.99

It is clear from the above table (3) that the results of the current method (FT-HPM) are in good agreement with the results of previous works.

7. Convergence Analysis of FT-HPM

This section presents some basic definitions and theorems that help in the study of convergence analysis. Moreover, the objective of this section is to find the necessary condition for convergence of approximate analytic solutions resulting from the application of the new algorithm (FT-HPM).

Definition 7.1 Let $\mathcal{T}: \mathbb{H} \longrightarrow \mathbb{R}$ be a non-linear mapping, where $\mathbb{H}$, $\mathbb{R}$ refers to the Banach space, the set of real numbers, respectively. Then, the sequence of the solutions can be written as

$$E_{n+1} = \mathcal{T}(E_n),\ E_n = \sum_{j=0}^{n} h_j,\ j = 0,1,2,3,\ldots \tag{74}$$

where, $\mathcal{T}$ satisfies the Lipschitz condition, such that for $\gamma \in \mathbb{R}$, we have

$$\|\mathcal{T}(E_n) - \mathcal{N}(E_{n-1})\| \leq \gamma \|E_n - E_{n-1}\|,\ 0 < \gamma < 1. \tag{75}$$

Theorem 7.1 The analytical-approximate solution series $\psi(r,\theta) = \sum_{j=0}^{\infty} \psi_j(r,\theta)$ that resulted from the application of the new algorithm (FT-HPM) converges if the following condition is proven:

$$\|E_{n+1} - E_n\| \to 0 \text{ as } n \to \infty \text{ for } 0 < \gamma < 1. \tag{76}$$

Proof:

$$\|E_{n+1} - E_n\| = \left\|\sum_{j=0}^{n+1} \psi_j - \sum_{j=0}^{n} \psi_j\right\| = \left\| \psi_0 + \sum_{j=1}^{n+1} \psi_j - \left[\psi_0 + \sum_{j=1}^{n} \psi_j\right] \right\|$$

$$= \left\| \psi_0 + \sum_{j=1}^{n+1} L_1^{-1}\left[\mathcal{H}_{j-1}\right] - \left\{\psi_0 + \sum_{j=1}^{n} L_1^{-1}\left[\mathcal{H}_{j-1}\right]\right\} \right\|$$

$$= \left\| \psi_0 + L_1^{-1} \sum_{j=1}^{n+1}\left[\mathcal{H}_{j-1}\right] - \left\{\psi_0 + L_1^{-1} \sum_{j=1}^{n}\left[\mathcal{H}_{j-1}\right]\right\} \right\|$$

Since, $E_{n+1} = \mathcal{T}(E_n)$, then

$$\|E_{n+1}-E_n\| = \left\|L_1^{-1}\mathcal{T}\sum_{j=0}^{n}[\mathcal{H}_{j-1}] - L_1^{-1}\mathcal{T}\sum_{j=0}^{n-1}[\mathcal{H}_{j-1}]\right\| = \| \; L_1^{-1}\mathcal{T}\left[\sum_{j=0}^{n}\psi_j\right] - L_1^{-1}\mathcal{T}\left[\sum_{j=0}^{n-1}\psi_j\right] \|$$

$$\leq |L_1^{-1}|\| \mathcal{T}\left[\sum_{j=0}^{n}\psi_j\right] - \mathcal{T}\left[\sum_{j=0}^{n-1}\psi_j\right] \| \leq \gamma\| \sum_{j=0}^{n} L_1^{-1}[\mathcal{H}_{j-1}] - \sum_{j=0}^{n-1} L_1^{-1}[\mathcal{H}_{j-1}] \|$$

$$\leq \gamma^2\left\|\sum_{j=0}^{n-1} L_1^{-1}[\mathcal{H}_{j-1}] - \sum_{j=0}^{n-2} L_1^{-1}[\mathcal{H}_{j-1}]\right\|$$

$$\vdots$$

$$\leq \gamma^n\left\|\sum_{j=0}^{1} L_1^{-1}[\mathcal{H}_{j-1}] - \sum_{j=0}^{0} L_1^{-1}[\mathcal{H}_{j-1}]\right\| = \gamma^n\|E_1-E_0\| \to 0 \text{ as } n\to\infty \text{ for } 0<\gamma<1.$$

Where,

$$L_1^{-1}(\cdot) = \mathcal{F}_2^{-1}\left[\frac{-1}{i\omega}\mathcal{F}_2\left(\mathcal{F}_1^{-1}\left[\frac{1}{i\omega}\mathcal{F}_1(\cdot)\right]\right)\right],$$

$$\mathcal{H}_{j-1} = \begin{bmatrix} \frac{\partial}{\partial t}\left(\frac{\partial^2\psi_{j-1}}{\partial r^2}\right)r + \frac{1}{r}\frac{\partial}{\partial t}\left(\frac{\partial^2\psi_{j-1}}{\partial\theta^2}\right) - \left(H^*_{j-1} - H_{j-1}\right) - \\ \left(\nabla^4\psi_{j-1}\right)r + Gr\left(rcos(\theta)\frac{\partial T_{j-1}}{\partial r} - sin(\theta)\frac{\partial T_{j-1}}{\partial\theta}\right) \end{bmatrix}.$$ ■

Theorem 7.2 The necessary condition for the convergence of the solutions series $T(r,\theta) = \sum_{j=0}^{\infty} T_j(r,\theta)$ that is generated by the current algorithm (FT-HPM), is to fulfill the following property:

$$\|E_{n+1}-E_n\| \to 0 \text{ as } n\to\infty \text{ for } 0<\gamma<1. \tag{77}$$

Proof:

$$\|E_{n+1}-E_n\| = \left\|\sum_{j=0}^{n+1} T_j - \sum_{j=0}^{n} T_j\right\| = \left\|T_0 + \sum_{j=1}^{n+1} T_j - \left[T_0 + \sum_{j=1}^{n} T_j\right]\right\|$$

$$= \left\| T_0 + \sum_{j=1}^{n+1} L_2^{-1}[\ddot{\mathcal{H}}_{j-1}] - \left\{T_0 + \sum_{j=1}^{n} L_2^{-1}[\ddot{\mathcal{H}}_{j-1}]\right\} \right\|$$

$$= \left\| T_0 + L_2^{-1}\sum_{j=1}^{n+1}[\ddot{\mathcal{H}}_{j-1}] - \left\{T_0 + L_2^{-1}\sum_{j=1}^{n}[\ddot{\mathcal{H}}_{j-1}]\right\} \right\|$$

Since, $E_{n+1} = \mathcal{T}(E_n)$, then

$$\|E_{n+1}-E_n\| = \| \; L_2^{-1}\mathcal{T}\sum_{j=0}^{n}[\ddot{\mathcal{H}}_{j-1}] - L_2^{-1}\mathcal{T}\sum_{j=0}^{n-1}[\ddot{\mathcal{H}}_{j-1}] \|$$

$$= \| \; L_2^{-1}\mathcal{T}\left[\sum_{j=0}^{n} T_j\right] - L_2^{-1}\mathcal{T}\left[\sum_{j=0}^{n-1} T_j\right] \| \leq |L_2^{-1}|\| \mathcal{T}\left[\sum_{j=0}^{n} T_j\right] - \mathcal{T}\left[\sum_{j=0}^{n-1} T_j\right] \|$$

$$\leq \gamma\| \sum_{j=0}^{n} L_2^{-1}[\ddot{\mathcal{H}}_{j-1}] - \sum_{j=0}^{n-1} L_2^{-1}[\ddot{\mathcal{H}}_{j-1}] \| \leq \gamma^2\| \sum_{j=0}^{n-1} L_2^{-1}[\ddot{\mathcal{H}}_{j-1}] - \sum_{j=0}^{n-2} L_2^{-1}[\ddot{\mathcal{H}}_{j-1}] \|$$

$$\vdots$$

$\leq \gamma^n \left\| \sum_{j=0}^{1} L_2^{-1}\left[\ddot{\mathcal{H}}_{j-1}\right] - \sum_{j=0}^{0} L_2^{-1}\left[\ddot{\mathcal{H}}_{j-1}\right] \right\| = \gamma^n \|E_1 - E_0\| \to 0$ as $n \to \infty$ for $0 < \gamma < 1$.

Where,

$L_2^{-1}(\cdot) = \mathcal{F}_2^{-1}\left[\frac{1}{i\omega}\mathcal{F}_2(\cdot)\right]$, $\ddot{\mathcal{H}}_{j-1} = \frac{1}{Pr}\nabla^2 T_{j-1} + \frac{1}{r}\left(G^*_{j-1} - G_{j-1}\right)$. ■

The results of theorems (7.1) and (7.2), can be used to calculate the values of the parameter γ^m by constructing the following definition.

Definition 7.2 For $m = 1,2,3, \ldots$

$$\gamma^m = \begin{cases} \frac{\|E_{m+1} - E_n\|}{\|E_1 - E_0\|} = \frac{\|h_{m+1}\|}{\|h_1\|}, \|h_1\| \neq 0, m = 1,2,3, \ldots \\ 0 \qquad\qquad\qquad\quad , \|h_1\| = 0 \end{cases} \tag{78}$$

To test the convergence of the analytical solutions to the current problem, we can use Eq. 78. Moreover, the convergence results of the analytical solutions calculated using two methods, FT-HPM and YT-HPM [2], were compared, and as listed in the Table 4:

Table 4. Comparison of powers of γ between FT-HPM and YT-HPM [2] at $Gr = 10$, $Pr = 0.7$, $t = 0.1$ and $R = 1.5$.

$\psi(r,\theta)$				$T(r,\theta)$			
Method	γ	γ^2	⋯	Method	γ	γ^2	⋯
FT-HPM	0.12×10^{-1}	0.33×10^{-4}	⋯	FT-HPM	0.30×10^{-3}	0.39×10^{-5}	⋯
YT-HPM	2.10×10^{-1}	0.60×10^{-2}	⋯	YT-HPM	0.57×10^{-2}	0.50×10^{-3}	⋯

From Table 4, we notice that $\gamma^n \to 0$ as $n \to \infty$ for $0 < \gamma < 1$, in addition, the difference in convergence can be observed between FT-HPM and YT-HPM, which shows that the powers of γ found by applying FLT-HPM approach zero faster than the powers of γ that were found based on YT-HPM. Accordingly, we find that FLT-HPM represents a better convergence than the YT-HPM.

8. Conclusions

In this article, a sophisticated analytical procedure is presented that combines the homotopy perturbation method with the Fourier transform to provide approximate analytical solutions to the problem of two-dimensional transient natural convection in a horizontal cylindrical concentric annulus bounded by two isothermal surfaces. The effect of radius ratio and Grashof number on heat transfer, fluid flow, velocity distribution, and Nusselt number was investigated. The effect of Grashof number for the range ($10^3 \leq Gr \leq 4 \times 10^4$), at three different radius ratios (1.2, 1.5, 2) in the case of $Pr = 0.7$ is discussed. We noticed through this study, the change in the flow pattern

and the temperature fields is almost very slight at $Gr = 10^3$ with different radius ratios, in addition to that the temperature pattern behaves like circles. When the Grashof number increases, the flow pattern moves up, while the temperature distribution pattern remains circles when the radius is small. On the other hand, the temperature distribution pattern is distorted with the increase in the radius ratio, which is a clear indication of the increase in convection. The results obtained based on the new algorithm FT-HPM agree with the previously published results. In addition, by discussing accuracy and efficiency, we concluded that FT-HPM represents a powerful and effective procedure that can be applied to solve many convection problems that have applications in various branches of science and engineering.

References

[1] A.M. Jasim, New Analytical Study for Nanofluid between Two Non-Parallel Plane Walls (Jeffery-Hamel Flow), J. Appl. Comput. Mech., 72 (2021) 13-224, https://doi.org/10.22055/jacm.2020.34958.2520.

[2] A.S.J Al-Saif, T.A. J Al-Griffi, Analytical Simulation for Transient Natural Convection in a Horizontal Cylindrical Concentric Annulus, J. Appl. Comput. Mech., 7 (2021) 621-637, https://doi.org/10.22055/jacm.2020.35278.2617.

[3] L. Crawford, R. Lemlich, Natural convection in horizontal concentric cylindrical annuli, Ind. Eng. Chem. Fundam, 1 (1962) 260-264, https://doi.org/10.1021/i160004a006.

[4] He J. H., Homotopy Perturbation Technique, Comput. Math. Appl. Mech. Engrg,. Vol.178, pp.257-262, (1999). https://doi.org/10.1016/S0045-7825(99)00018-3.

[5] J.H He, A coupling method of a homotopy technique and a perturbation technique for non-linear problems. Int. J. of Non-Linear Mech., 35(2000)37-43 https://doi.org/10.1016/S0020-7462(98)00085-7.

[6] J.H He, The homotopy perturbation method for nonlinear oscillators with discontinuities. Appl. Math. Comput., 15(2004) 287-292, https://doi.org/10.1016/S0096-3003(03)00341-2.

[7] A Hassan, J. Al-Lateef, Numerical simulation of two-dimensional transient natural convection heat transfer from isothermal horizontal cylindrical annuli, Eng. Technolo. J, 25 (2007) 728-745, https://search.emarefa.net/detail/BIM-52805.

[8] T. Kuehn, J. Goldstein, An experimental and theoretical study of natural convection in the annulus between horizontal concentric cylinders, J Fluid Mech.,74(1976)695-719, https://doi.org/10.1017/S0022112076002012.

[9] R. Lawrence, E. Mack, H. Bishop, Natural Convection Between Horizontal Concentric Cylinders for Low Rayleigh Numbers, Quat. J. Mech. Appl. Math., 2 (1968)223-241 https://doi.org/10.1093/qjmam/21.2.223

[10] H.M Meisam, M. Omid, W. Somchai, Nanofluids Flow Between Two Rotating Cylinders: Effects of Thermophoresis and Brownian Motion, J Thermo Phys Heat Trans., 10(2013)1-8 https://doi.org/10.2514/1.T4122.

[11] M. Medebber, N. Retiel, B. Said, Aissa A. and El-Ganaoui M., Transient Numerical Analysis of Free Convection in Cylindrical Enclosure, MATEC Web of Conferences, 307(2020)1-9, http://dx.doi.org/10.1051/matecconf/202030701029.

[12] I. Pop, D. Ingham, P. Cheng, Transient natural convection in a horizontal concentric annulus filled with a porous medium, J Heat Trans., 114, (1992) 990-997, https://doi.org/10.1115/1.2911911.

[13] S. Dinarvand, R. Hosseini, and I. Pop, Homotopy analysis method for unsteady mixed convective stagnation-point flow of a nanofluid using Tiwari-Das nanofluid model, Int. J Num., 16(2016)40-62, https://doi.org/10.1108/HFF-12-2014-0387

[14] C. Shu, H. Xue, Y.D Zhu, Numerical study of natural convection in an eccentric annulus between a square outer cylinder and a circular inner cylinder using DQ method, International J Heat Mass Trans., 44 (2001) 3321-3333, https://doi.org/10.1016/S0017-9310(00)00357-4.

[15] S. Sushila, Y.S Shishodia,, A reliable approach for two-dimensional viscous flow between slowly expanding or contracting walls with weak permeability using sumudu transform. Ain Shams Eng. J, 5(2014) 237-242, https://doi.org/10.1016/j.asej.2013.07.001.

[16] C. Shu, Y.D Zhu, Efficient computation of natural convection in a concentric annulus between an outer square cylinder and an inner circular cylinder, Int. J. Numer. Meth. Fluids; 38(2002) 429–445, https://doi.org/10.1002/fld.226.

[17] Y.T Tsui, B. Trembaly, On Transient Natural Convection Heat Transfer in the Annulus between Convective, Horizontal Cylinders with Isothermal Surfaces", Int. J. Heat Mass Trans, 27 (1983) 103-111, https://doi.org/10.1016/0017-9310(84)90242-4.

[18] S. Touzani, A. Cheddadi, M. Ouazzani, Natural Convection in a Horizontal Cylindrical Annulus with Two Isothermal Blocks in Median Position: Numerical Study of Heat Transfer Enhancement, J. Appl. Fluid Mech., 13(2020) 327-334, https://doi.org/10.29252/jafm.13.01.30082.

[19] L. Zhang, Y. Hu, M. Li M., Numerical Study of Natural Convection Heat Transfer in a Porous Annulus Filled with a Cu-Nanofluid, Nanomaterials, 11 (2021)990-1013, https://doi.org/10.3390/nano11040990.

أسلوب تقريبي تحليلي هجين لحل الحمل الحراري الطبيعي في أسطوانات أفقية متحدة المركز

ياسر احمد عبد الأمير،عبد الستار جابر السيف

قسم الرياضيات، كلية التربية للعلوم الصرف، جامعة البصرة، العراق

المستخلص

تم اقتراح إجراء هجين يجمع طريقة الاضطراب الهوموتوبي مع تحويل فوريه، وقد تم استخدام هذا الإجراء لإيجاد حل تحليلي تقريبي لمشكلة الحمل الحراري الطبيعي العابر ثنائي الأبعاد في حلقة أفقية أسطوانية متحدة المركز يحدها سطحان متساويا الحرارة. تمت مناقشة تأثير رقم Grashof ورقم Prandtl ونسبة نصف القطر على تدفق السوائل (الهواء) ونقل الحرارة بقيم مختلفة. علاوة على ذلك، تم دراسة توزيعات السرعة ومتوسط عدد نسلت، حيث تم استخدام أرقام نسلت للتعبير عن معدلات انتقال الحرارة المحلية والعامة. أخيرًا، تم اختبار تقارب الخوارزمية الجديدة نظريًا من خلال إثبات بعض النظريات، بالإضافة إلى تطبيق هذه النظريات على نتائج الحلول الجديدة التي تم الحصول عليها بالطريقة المقترحة.